Provided for non-commercial research and education use.
Not for reproduction, distribution or commercial use.

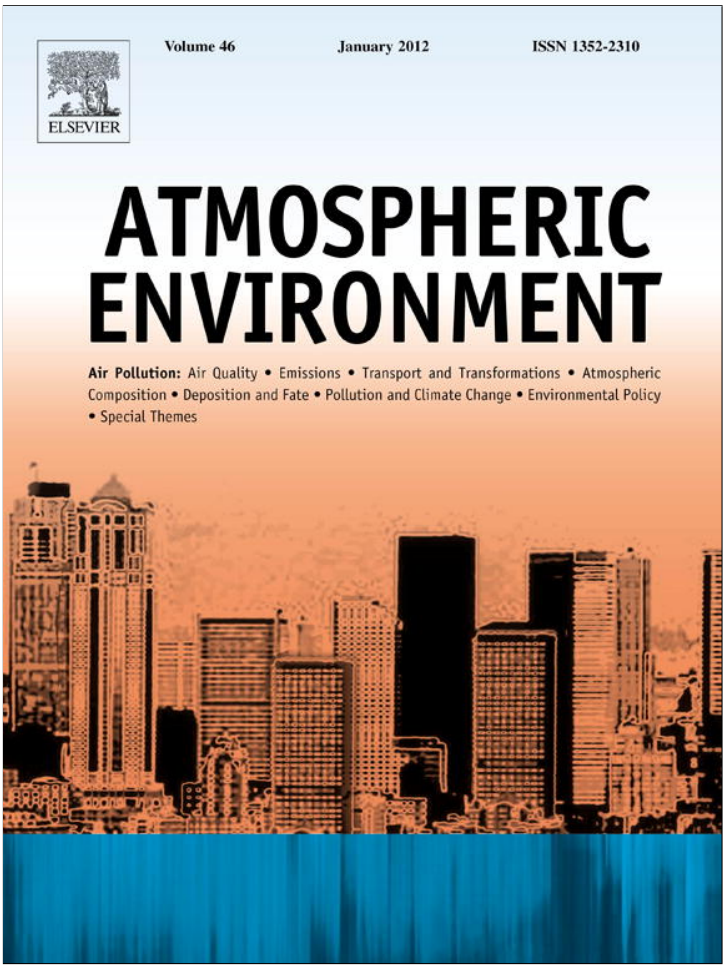

(This is a sample cover image for this issue. The actual cover is not yet available at this time.)

This article appeared in a journal published by Elsevier. The attached copy is furnished to the author for internal non-commercial research and education use, including for instruction at the authors institution and sharing with colleagues.

Other uses, including reproduction and distribution, or selling or licensing copies, or posting to personal, institutional or third party websites are prohibited.

In most cases authors are permitted to post their version of the article (e.g. in Word or Tex form) to their personal website or institutional repository. Authors requiring further information regarding Elsevier's archiving and manuscript policies are encouraged to visit:

http://www.elsevier.com/copyright

Author's personal copy

Atmospheric Environment 54 (2012) 373–386

Contents lists available at SciVerse ScienceDirect

Atmospheric Environment

journal homepage: www.elsevier.com/locate/atmosenv

A backward-time stochastic Lagrangian air quality model

Deyong Wen [a,*], John C. Lin [a], Dylan B. Millet [b], Ariel F. Stein [c], Roland R. Draxler [c]

[a] Waterloo Atmosphere–Land Interactions Research Group, Department of Earth and Environmental Sciences, University of Waterloo, 200 University Avenue West, Waterloo, Ontario, Canada N2L 3G1
[b] Department of Soil, Water and Climate, University of Minnesota, USA
[c] National Oceanic and Atmospheric Administration, Air Resources Laboratory, Silver Spring, MD, USA

ARTICLE INFO

Article history:
Received 8 October 2011
Received in revised form
9 February 2012
Accepted 11 February 2012

Keywords:
Air quality
Lagrangian model
Cross-border pollutant transport
Tropospheric ozone

ABSTRACT

We describe a backward-time Lagrangian air quality model based on time-reversed, stochastic particle trajectories. The model simulates the transport of air parcels backward in time using ensembles of fictitious particles with stochastic motions generated from the Stochastic Time-Inverted Lagrangian Transport model (STILT). Due to the fact that STILT was originally developed out of the HYSPLIT lineage, the model leverages previous work (Stein et al., 2000) that implemented within HYSPLIT a chemical scheme (CB4). Chemical transformations according to the CB4 scheme are calculated along trajectories identified by the backward-time simulations. This approach opens up several key advantages: 1) exclusive focus upon air parcels that affect the receptor's air quality; 2) the separation of transport processes—elucidated by backward-time trajectories—from chemical reactions that enables implications of multiple emission scenarios to be probed; 3) the potential to incorporate detailed sub-gridscale mixing and transport phenomena that are not tied to Eulerian gridcells.

The model was used to simulate concentrations of air quality-relevant species (O_3 and NO_x) at eight measurement sites in the Canadian province of Ontario. The model-predicted concentrations were compared with observations, and comparisons show that simulated O_3 concentrations usually agree well with observations across sites in rural areas, small towns, and big urban regions. Furthermore, the backward-time model showed improved performance over the previous approach involving forward-time particle trajectories, especially for O_3. However, the model under-estimated NO_x at sites away from the big cities, possibly due to the inability of the coarsely gridded emission grids to resolve fine-scale NO_x sources.

Influences of cross-border transport of U.S. emission sources on the test sites were investigated using the model by turning off anthropogenic and natural U.S. emission sources. The model results suggest that total U.S. emissions contributed more than 30% of O_3 concentrations at the target sites and that over half of all hours during the simulation period were affected either by anthropogenic or natural emissions from the U.S. sources, indicating the importance of U.S. sources for air quality across Ontario.

© 2012 Elsevier Ltd. All rights reserved.

1. Introduction

Anthropogenic emissions of chemically active species are altering the composition of the atmosphere and will become increasingly important over the next decades (Brasseur et al., 1999; Crutzen and Ramanathan, 2000). Biomass burning from land use change has been accelerating (Setzer et al., 1994), releasing large quantities of NO_x ($NO + NO_2$) and volatile organic compounds (VOC) to the atmosphere (Chatfield and Delany, 1990). In the developing world, regional scale air pollution will accelerate from urbanization and industrialization, leading to human health problems and crop damage (Chameides et al., 1994, 1999). After being emitted, such pollutants are mixed in the atmosphere and transported across borders (Brankov et al., 2003), resulting in regional scale pollution that can be examined quantitatively only with models that account for chemistry and transport at the appropriate scales. In developed nations, the adverse effects of air pollution on human health continue to be observed—e.g., increased respiratory hospitalization in Windsor, Ontario (Luginaah et al., 2005; Malig and Ostro, 2009). Such human health concerns have led to increasingly stringent controls on air quality by the U.S. EPA (1997) and the Canadian Council of Ministers of the Environment (2000)

* Corresponding author.
E-mail address: dwen@scimail.uwaterloo.ca (D. Wen).

1352-2310/$ – see front matter © 2012 Elsevier Ltd. All rights reserved.
doi:10.1016/j.atmosenv.2012.02.042

Author's personal copy

that necessitate careful balances between health benefits and mitigation costs (Pandey and Nathwani, 2003; Russell, 1988). Societal concerns regarding the anthropogenic impact on atmospheric chemistry and air quality call for improvements to modeling and analysis of regional scale atmospheric chemistry (Russell and Dennis, 2000).

A variety of numerical air quality models have been developed since the 1970s. Such models are broadly classified into two types according to whether they adopt Lagrangian or Eulerian coordinate systems. Eulerian models calculate the pollutant's fate and transport everywhere in the modeling domain using a fixed coordinate system. Lagrangian models calculate the trajectories of air parcels and follow them as they move through the model domain (Lin et al., 2011).

Eulerian models are powerful tools for elucidating the chemical and physical mechanisms in the atmosphere. Current generation atmospheric chemistry models generally adopt an Eulerian approach. However, Eulerian models calculate chemical reactions usually based on pollutant concentrations diluted over entire gridcells. The artificial dilution likely results in under-prediction of concentrations (Gillani and Pleim, 1996). Numerical diffusion introduced by space discretization in Eulerian models also imposes artificial mixing of pollutants (Jacobson, 1998; Odman, 1997). Advances in regional chemical modeling require further improvements in incorporating atmospheric transport processes other than mixing. Processes such as turbulent fluctuations in tracer concentrations (Fitzjarrald and Lenschow, 1983; Georgopoulos and Seinfeld, 1986), boundary-layer top entrainment (Davis et al., 1997), and convective transport (Thompson et al., 1994) remain difficult to represent in the sub-grid scale eddy diffusion coefficient approach adopted by most Eulerian models. Moreover, the grid-averaged concentrations prognosed by gridded models are difficult to compare with point observations.

Lagrangian models have the key advantage of being subject to minimal numerical diffusion (Seibert, 2004). Backward-time Lagrangian approaches are also computationally cheap, because Lagrangian air parcel trajectories running backward from the receptor site isolate the upwind influences on the receptor. Various Lagrangian approaches have been adopted for photochemical modeling in an attempt to complement and address limitations in Eulerian methods. The simplest of these Lagrangian models simulates pollutants within boxes that are advected along mean wind trajectories (Eliassen et al., 1982; Simpson, 1993). However, the idealized box representation cannot readily incorporate detailed transport processes. Alternatively, puff models such as CALPUFF (Scire et al., 2000) represent pollutant emissions with Gaussian puffs that attempt to simulate dispersion effects. However, puff models have difficulties capturing the interaction between turbulence and wind shear which distort plumes into non-Gaussian shapes, potentially introducing large biases in the peak concentrations and the plume area, thereby requiring ad hoc parameterizations such as puff splitting (Walcek, 2002; Draxler and Taylor, 1982).

Out of all of the Lagrangian approaches, stochastic particle models are the most sophisticated (Stohl, 1998). These models have the capability to simulate complicated transport effects—e.g., wind shear, convective redistribution, and turbulent dispersion. Of particular importance for stochastic particle models are simulations of transport within the planetary boundary layer (PBL), in the lower troposphere, where strong turbulence renders single deterministic mean wind trajectories highly erroneous (Stohl and Wotawa, 1995). Since ground-based air quality monitoring sites are necessarily located within the PBL, a strong need exists for the Lagrangian particles to be stochastic in nature and run backward in time, to take advantage of the aforementioned computational savings.

Stein et al. (2000) developed a stochastic Lagrangian model that runs forward in time. Recently, Miller et al. (2008) and Wen et al. (2011) described the use of backward-time stochastic trajectories to simulate air quality-relevant species. However, chemistry was neglected or highly-simplified in those studies.

In this paper, we developed a comprehensive Lagrangian air quality model based upon the backward-time stochastic Lagrangian approach. The new model is capable of simulating a wide variety of gas phase species that affect air quality using the Carbon Bond IV (CB4) mechanism (Gery et al., 1989). Lin et al. (2003) have demonstrated that given proper formulation of turbulent transport and mass conserving meteorological fields, backward-time results are identical to their forward-time analogs. In other words, backward-time simulations retrieve the trajectories of all air parcels arriving at the receptor in the forward-time case. This means that the backward-time air parcels—and only these parcels—contribute to variations in chemical tracers at the receptor, and these parcels isolate the region of the model domain needed to be accounted for in the chemical simulations. The chemical calculations can then be conducted forward in time from the regions marked out by these particles and along their trajectories, taking into account surface emissions, chemical transformations, and mixing processes.

This approach opens up several key advantages: 1) exclusive focus upon air parcels that affect the receptor's air quality; 2) the separation of transport processes elucidated by backward-time trajectories from chemical reactions, enabling implications of multiple emission scenarios to be probed ("reusing" transport information to achieve computational efficiency); 3) the potential to incorporate detailed sub-gridscale mixing and transport phenomena that are not tied to Eulerian gridcells.

It bears mentioning that 3) above is only a potential that may be realized in the future with the approach presented in this paper. Currently the particles' concentrations are mixed and averaged over fixed Eulerian grids to simulate chemical transformations, following a "hybrid Lagrangian-Eulerian" approach that has been introduced by others already (Stein et al., 2000; Stevenson et al., 1998).

The model is designed to simulate air quality over scales of 10–1000 km, serving as a crucial bridge at the regional scale, between coarse-scale global models and the fine-scale large-eddy simulations or urban air-shed models. As a test and initial application of the model, it was applied to simulate air concentrations of tracers at eight measurement sites in Ontario, Canada (Sect. 4.2). A comparison with the forward-time approach was also carried out. As an application of the model, the impact of cross-border transport of U.S. emission on Ontario was investigated (Sect. 4.3). This is an important policy and health question for Canada, as a significant fraction of the Canadian population resides near the U.S. border, downwind of numerous cities, power plants, and other large pollution sources (CEC, 2004).

2. Model description

2.1. Overview

The backward-time stochastic Lagrangian air quality model was developed from the Stochastic Time-Inverted Lagrangian Transport Model (STILT; see http://www.stilt-model.org) (Lin et al., 2003). STILT was built from the Hybrid Single-Particle Lagrangian Integrated Trajectory (HYSPLIT) model (Draxler and Hess, 1997). STILT was originally developed for atmospheric transport simulations of inert tracers, especially greenhouse gases (Gourdji et al., 2010; Zhao et al., 2009; Kort et al., 2008). Recently, efforts have been made to simulate air quality-relevant species using the STILT model (Miller et al., 2008; Wen et al., 2011). However, chemistry was neglected or highly simplified in those studies. This paper represents further development to account for chemical transformations of a wide

Author's personal copy

variety of species that affect air quality. This development leverages off of earlier work by Stein et al. (2000), which coupled the CB4 chemical mechanism (see Sect. 2.4 below) to HYSPLIT.

The air quality simulation (Fig. 1) begins with a stochastic back-trajectory simulation, followed by a forward chemical simulation that determines tracer concentrations along the generated back trajectories. In the back-trajectory simulation, numerous particles, each representing an air parcel, are released from a receptor and transported backward in time for a specific period. Each particle is transported with both interpolated windfields as well as stochastic velocities representing turbulent eddies. After back trajectories are calculated, the concentrations of modeled species are initialized at the endpoint of each back-trajectory using values outputted from a global chemical transport model (Sect. 3.2.1). Then the concentrations are evolved forward in time along each trajectory to take into consideration the influences of emission, deposition, mixing and chemical transformation. Advection, diffusion, emission and deposition in the model are computed in a Lagrangian framework while chemistry is calculated on a fixed grid using a particle-in-grid method (Chock and Winkler, 1994; Stein et al., 2000). Particles within each gridcell are assumed to be uniformly mixed before chemical transformation and after that the resulting concentrations are redistributed among all particles located in that gridcell (Sect. 2.6). Concentrations at the receptor are obtained by averaging the concentrations of all particles arriving at the receptor.

2.2. Transport

This model uses STILT to simulate the transport of air parcels, represented as fictitious particles. Each fictitious particle is advected with mean wind velocities as well as stochastic velocities parameterized to capture the effect of turbulent transport. The effect of the turbulence is modeled by adding a random velocity to the mean motion for each particle. This random velocity is a function of the turbulence intensity and is different for each particle. To satisfy the well-mixed criterion (Thomson, 1987) in the strongly inhomogeneous environment of the PBL where the simple drift correction does not work (Lin et al., 2003; Thomson et al., 1997), a reflection/transmission scheme for Gaussian turbulence was employed. The parameterization for the PBL height was a modified Richardson number method that generalizes to unstable, neutral, and stable conditions (Lin et al., 2003; Vogelezang and Holtslag, 1996). The treatment of transport and dispersion in STILT has been described in detail by Lin et al. (2003) and Draxler and Hess (1997).

The transport of particles is simulated backward in time by this model. The backward mode is computationally advantageous if the number of receptors is less than the number of sources considered. Thought of another way, these particles are a means to determine the trajectories and to probe the processes experienced by substances in their transport history.

2.3. Emission

The concentration change of a species due to surface emissions is calculated using a "footprint" concept. A footprint $f(\vec{x}_r, t_r | x_i, y_j, t_m)$, calculated in a back-trajectory simulation, in units of ppm (μmole m^{-2} s^{-1})$^{-1}$, represents the sensitivity of the mixing ratio arriving at its receptor at location $\vec{x}_r$ at time t_r to the surface flux $F(x_i,y_j,t_m)$ from location x_i,y_j at time t_m. Thus it is a measure of the contribution from a source of unit strength located at x_i,y_j at time t_m to the mixing ratio at the receptor. The footprint is derived from the local density of particles by counting the number of particles (out of total number N_{tot}) in surface-influenced boxes and determining the amount of time $\Delta t_{p,i,j,k}$ each particle p spends in each surface volume element (i,j,k) during each time step. The mathematical definition of a footprint (Lin et al., 2003) is given by:

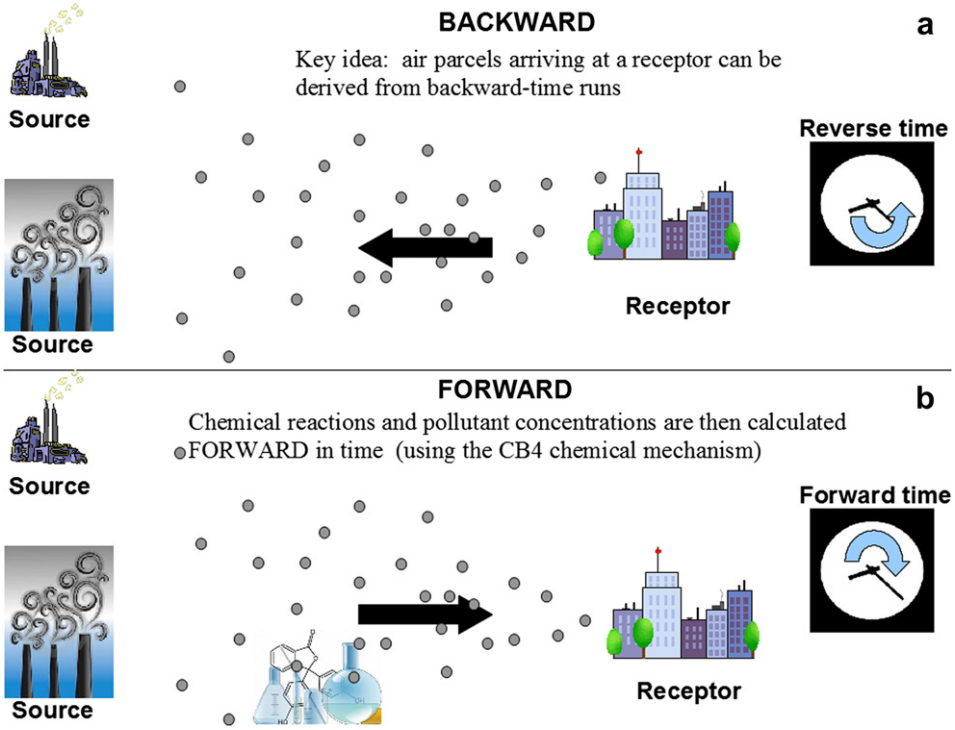

Fig. 1. Schematic representing the two steps of the air quality simulation: a) a backward-time stochastic Lagrangian particle simulation to describe atmospheric transport; b) chemical calculations forward in time, along the back-trajectory.

Author's personal copy

$$f\left(\vec{x}_r, t_r \middle| x_i, y_j, t_m\right) = \frac{m_{\text{air}}}{h\overline{\rho}\left(x_i, y_j, t_m\right)} \frac{1}{N_{\text{tot}}} \sum_{p=1}^{N_{\text{tot}}} \Delta t_{p,i,j,k} \quad (1)$$

where m_{air} is the molar mass of air, h is the height below which turbulent mixing is strong enough to mix the surface flux thoroughly, and $\overline{\rho}(x_i, y_j, t_m)$ is the average air density below h.

The concentration change $\Delta C_{m,i,j}(s,p,t_r)$ of the sth species in the p th particle arriving at its receptor at time t_r due to a surface emission flux $F(x_i,y_j,t_m)$ (μmole m^{-2} s^{-1}) is incremented whenever the parcel dips below a specific height h which is determined in STILT as a fraction of the PBL height (Lin et al., 2003). The fraction was set to 0.5 in this study. The concentration change is then given by:

$$\Delta C_{m,i,j}(s,p,t_r) = f\left(\vec{x}_r, t_r \middle| x_i, y_j, t_m\right) F\left(x_i, y_j, t_m\right) \quad (2)$$

This footprint formulation is applied for emission sources at the surface. For emissions at altitude (e.g., smokestacks) we dilute the source thoroughly in each emission gridcell in which the pth particle is found during one model time step (Wen et al., 2011):

$$\begin{aligned}\Delta C_{m,i,j,k}(s,p,t_r) &= \frac{D\left(x_i,y_j,z_k,t_m\right)}{N_{\text{tot}}} \sum_{p=1}^{N_{\text{tot}}} \Delta t_{p,i,j,k} \\ &= F\left(x_i,y_j,z_k,t_m\right) \frac{m_{\text{air}}}{L\overline{\rho}\left(x_i,y_j,z_k,t_m\right)} \frac{1}{N_{\text{tot}}} \sum_{p=1}^{N_{\text{tot}}} \Delta t_{p,i,j,k}.\end{aligned} \quad (3)$$

Where $F(x_i,y_j,z_k,t_m)$ is the emission flux in a grid box (i,j,k) at time t_m. $D(x_i,y_j,z_k,t_m)$ represents the dilution of emission flux in the grid box with a height of L.

2.4. Gas phase chemistry

The chemical mechanism used in this model is based on the Carbon Bond IV (CB4) Mechanism (Gery et al., 1989). The CB4 mechanism is a collection of reactions that transforms reactants into products, including key intermediates, developed primarily to simulate urban and regional ozone formation. The mechanism used here contains 94 reactions and 39 chemical species. We updated all rate constants according to the values reported by Yarwood et al. (2005). The resulting system of stiff ordinary differential equations of the mechanism is solved using a modified Gear method (Gear, 1971; Press et al., 1992; Spellmann and Hindmarsh, 1975). The Gear solver is an implicit, backwards difference algorithm in which concentrations from previous time steps are used to predict the concentration at the current time. The algorithm automatically adjusts the size of the time step and the order (the number of previous time steps used) to optimize the solution. The algorithm also estimates the error in the numerical solution at each time step, and the user can specify an error tolerance that constrains the accuracy of the solution. The photolysis rate constants needed to calculate the chemical transformations are computed as a function of the solar zenith angle, cloud cover, and chemical species for each particle at each time step.

The model is designed to take as input user-specified chemical species and reactions, emissions, deposition parameters. This allows considerable flexibility in specifying chemical mechanism, emissions, and deposition parameters and output variables.

2.5. Deposition

Dry and wet deposition are treated in a similar way as described by Wen et al. (2011). Accordingly, the concentration change of the sth species in a particle due to dry and wet deposition is expressed in terms of time constants:

$$\frac{dC_s}{dt} = -\left(\beta_{d_s} + \beta_{w_s}\right) C_s \quad (4)$$

where β_{d_s} and β_{w_s} are time constants for dry and wet deposition for the sth species respectively. The time constant for dry deposition can be expressed as:

$$\beta_{d_s} = \frac{V_{\text{dry}_s}}{Z_s} \quad (5)$$

where V_{dry_s} (cms^{-1}) is the dry deposition velocity for the sth species. The dry deposition velocities can be either calculated using a resistance-in-series scheme (Wesely, 1989; Draxler and Hess, 1997) by this model, or provided explicitly. In this work, the dry deposition velocities were calculated explicitly by a separate model (Sect. 3.2.2). Dry deposition is only estimated when a particle moves into the lowest model level, the depth of which (Z_s) is approximately 50 m, and is assumed to be the top of the surface layer.

Wet deposition is represented via loss rates computed based on the large-scale and convective precipitation rates. The wet deposition of gases depends upon their solubility. The influences of aqueous phase reactions are assumed negligible and are not considered in this work. For non-reactive gases the wet deposition is a function of the effective Henry's Law constant. The gaseous wet deposition velocity for the sth species can be defined as (Draxler and Hess, 1997):

$$V_{\text{wet}_s} = H_s RTP \quad (6)$$

where R is the universal gas constant (0.082 atm mol^{-1}K^{-1}L) and T and P are, respectively, air temperature and precipitation rate in a particle. H_s is the effective Henry's Law constant of the sth species. Gaseous wet removal only occurs for the fraction of the pollutant below the cloud top. The gaseous wet removal time constant is given by:

$$\beta_{w_s} = \frac{F_t V_{\text{wet}_s}}{Z_p} \quad (7)$$

where Z_p is the depth of the meteorological layer in which the particle is found. F_t is the fraction of the layer that is below the cloud top.

2.6. Mixing parameterization

Since the model presented here uses the particle-in-grid approach to simulate chemistry, uniform mixing of particles in each gridcell is assumed and conducted before the chemical transformations are performed. The meteorological grid is used as the default grid for particle mixing and chemistry. That means particles are well mixed in each cell of the meteorological grid, and each cell is treated as a reactor.

After the chemical transformations have been calculated, the resulting concentrations are then used to update the concentration of each chemical compound in each particle following the method from Stein et al. (2000).

3. Model simulation

3.1. Measurement sites used for simulation and comparison

Eight measurement sites in Ontario, Canada, were selected as receptors in the model simulations (Fig. 2). These eight sites were selected mainly to investigate the cross-border transport and the

Author's personal copy

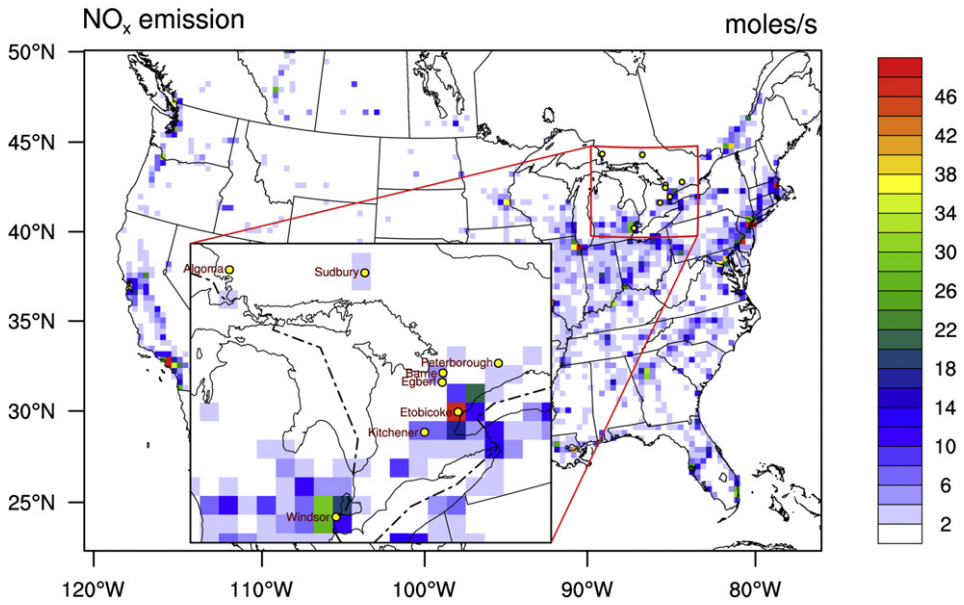

Fig. 2. Locations of eight measurement sites and their local NO_x emission rates averaged over the simulation period.

contrast between rural and urban air pollutant levels in southern Ontario. Details regarding the eight sites can be found in Table 1. Six of them—Windsor, Etobicoke, Sudbury, Peterborough, Barrie and Kitchener—are from The National Air Pollution Surveillance (NAPS) Network. NAPS is primarily an urban network, gathering measurements on O_3, PM, SO_2, CO, NO_x and volatile organic compounds (VOCs). VOCs were not measured at all those sites for 2002, which is the year this study was focused on. Windsor, Kitchener, Etobicoke and Peterborough are located from southwest to northeast along the main population corridor in Ontario while Etobicoke, Barrie, Sudbury, and Algoma represent a south to north gradient that coincides with a decline in population density. Windsor and Etobicoke are found in big urban areas. Windsor is across the Detroit River from the U.S. city of Detroit, Michigan. Etobicoke is situated in the Greater Toronto Area, the most populous metropolitan area in Canada with over 5 million people. Egbert and Algoma are two sites from the Canadian Air and Precipitation Monitoring Network (CAPMoN), a rural network with 10 air monitoring stations across Canada. CAPMoN measurements are regionally representative and less affected by local sources of air pollution. Only O_3 measurements are available for these two sites from CAPMoN. Egbert is less than 20 km away from the Barrie site, providing a contrast between rural and urban observations in a similar geographical region.

3.2. Base case simulation

The model was used to simulate air pollutant concentrations at the eight sites for ten days from July 20th to July 29th in 2002. The simulations were driven by meteorological data from the NCEP North American Regional Reanalysis (NARR) (Mesinger et al., 2006). The NARR data have 239 × 277 grids with a horizontal resolution of 32 km covering all of North America. The data cover 45 vertical layers and are available at three-hourly intervals. In the simulations, ensembles of 1000 particles were released from each site location every hour. The choice of 1000 particles will be explained in Sect. 4.1. These particles were run backward in time for six days, which usually allowed them to be far away from any sources near the receptors.

Table 1
Information regarding the eight measurement sites in this study.

Site	Latitude (°)	Longitude (°)	Instrument height (m)	Type
Windsor	42.316021	−83.043817	8.0	Urban
Etobicoke	43.64852	−79.59138	5.0	Urban
Sudbury	46.46847	−80.98958	10.0	Urban
Peterborough	44.30733	−78.32071	7.0	Urban
Kitchener	43.44183	−80.50446	5.0	Urban
Barrie	44.39222	−79.70417	5.0	Urban
Egbert	44.23250	−79.78139	5.0	Rural
Algoma	47.03500	−84.38111	5.0	Rural

3.2.1. Initial/Boundary conditions

At the endpoints of particles, concentrations of modeled species were initialized using monthly mean output for 2002 from a global, 3-D chemical transport model (GEOS-Chem; http://www.geos-chem.org), according to the spatial locations of particles' endpoints in the GEOS-Chem simulation domain. The GEOS-Chem simulation (Millet et al., 2010) was carried out with 2° latitude by 2.5° longitude (2° × 2.5°) grid spacing on 48 sigma vertical layers. The monthly output of the simulation was interpolated to each day using the Aitken interpolation method (Aitken, 1932) to represent daily variation in the concentration initialization. Since chemical species used in GEOS-Chem are different from those in CB4, chemical species in GEOS-Chem were mapped onto CB4 species according to the match table given by Lam and Fu (2009). After the initialization, the simulation is performed forward in time to simulate the evolution of concentration due to the influence from emission, chemical reactions and deposition along each trajectory for each time step.

3.2.2. Dry deposition velocities and emission datasets

Values of dry deposition velocities and emission datasets prepared for 2002 for a previous study (Gbor et al., 2007) were directly employed in this work. The dry deposition velocities were calculated by the Meteorology–Chemistry Interface Processor (MCIP) using the Models-3/CMAQ Dry Deposition Model (Byun et al., 1999). The emissions come from a SMOKE-processed emission dataset having 132 × 90 gridcells with a horizontal spacing of 36 km and 15 vertical layers. The 1999 National Emission Inventory (NEI) version 3 IDA Files (U.S. EPA, 2004) were used for emissions of anthropogenic pollutants in the United States and a 1995 inventory

Author's personal copy

over Canada from the Ontario Ministry of Environment (OMOE) (Chtcherbakov, 2003). Emissions of pollutants from biogenic sources were processed using the BEIS3 program of the Sparse Matrix Operator Kernel Emission (SMOKE) modeling system. We incorporated the Models-3 Input/Output Application Programming Interface (IOAPI) (Coats, 2003) into the model presented here so that the model can read in emissions directly from SMOKE output in the simulation.

3.3. Scenarios

To investigate the source contributions from the United States to air quality in Ontario, the model was also run for the following three scenarios in addition to the base run:

1. No U.S. natural emissions: same as base case but all U.S. natural emission sources (e.g., vegetation and soils) were turned off.
2. No U.S. anthropogenic emissions: same as base case but all U.S. anthropogenic emission sources (e.g., electric generating utilities, chemical manufacturers, furniture refinishers, vehicles, residential heating, and waste landfill) were turned off.
3. No U.S. emissions: same as base case but all U.S. emissions (anthropogenic + natural) were turned off.

4. Results

4.1. Sensitivity to particle number

Due to the stochastic nature of particle trajectories, the accuracy of the model's simulation is affected by the number of particles used. An infinite number of particles is theoretically required to completely represent the ensemble properties of transport to a given measurement location. In reality, however, only a limited number of particles can be used in a simulation due to finite computational resources. This leads to incomplete sampling of trajectory pathways and emissions, resulting in fluctuations in simulated concentrations. A small particle number can reduce computing time significantly. To find the appropriate number of particles in a simulation that can achieve adequate accuracy while also reducing computational time, we ran the model with different particle numbers for the Barrie measurement site. The particle numbers examined include 10, 20, 50, 100, 150, 1000, 2000 and 3000, and simulated O_3 time series are presented in Fig. 3. The results show that simulated concentrations with a small particle number are more variable than those with a big number. Discrepancies between simulations with small and large numbers of particles are significant. When the particle number is larger than 1000, modeled concentrations become close and almost overlap each other. The larger the particle number, the closer the values approach the modeled values with 3000 particles. Therefore, we assumed that the modeled results with 3000 particles act like "true values" without error caused by insufficient particles. Fig. 3 also shows the deviations of all simulations away from the simulation with 3000 particles where the discrepancy is calculated as the Mean Normalized Gross Error (MNGE, defined in Table 2). Since the model run time is proportional to the number of particles, we chose 1000 particles for use in the present simulations, which yielded an MNGE less than 5% compared to a run with 3000 particles.

4.2. Model performance evaluation

Model performance was also evaluated with measurements for all test sites by using three model performance metrics recommended by U.S. EPA (1991): the unpaired peak accuracy (UPA), the mean normalized gross error (MNGE) and the mean normalized bias error (MNBE). Their definitions are listed in Table 2. MNBE and MNGE indicate the overall performance of the model while UPA represents the model's ability to simulate the peak concentrations.

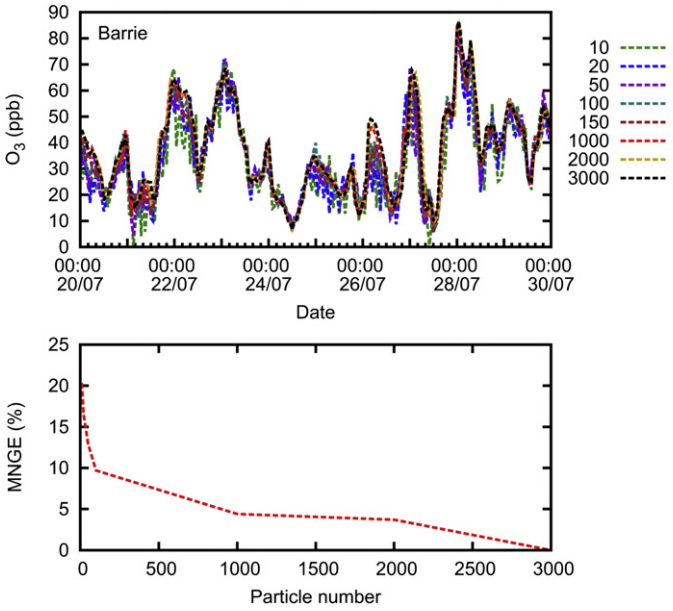

Fig. 3. Sensitivity of the model simulation to the number of particles: including modeled O_3 concentrations at Barrie with different particle numbers (Top) and deviations (MNGEs) of O_3 from the simulation with 3000 particles (Bottom).

4.2.1. Ozone (O_3) results

Model-simulated hourly O_3 concentrations were compared with measurements for all test sites during the simulation period from July 20th to 29th, 2002. The comparison results (in Fig. 4) show that the model performed well in predicting O_3 concentrations at all sites: the model captured the general variability in the measurements, the timing of peaks, and the diurnal cycle.

Summary metrics and statistical measures for 1-h O_3 concentration for all the sites are presented in Table 3. EPA guidance (U.S. EPA, 1991) recommends using MNGE and MNBE for O_3 model performance evaluations in conjunction with an observation-based minimum threshold. An observation-based minimum threshold is required since the normalized quantities can become large when the observations are small. EPA modeling guidance recommends using a cut-off value of 60 ppb (U.S. EPA, 2007); however, this cut-off would eliminate most of the observations for some sites (Sudbury) in our model performance evaluation. In this study, a cut-off value of 40 ppb was used, and the MNGE and MNBE statistical measures were calculated using all predicted and observed hourly O_3 pairs matched by time for which the observed O_3 was 40 ppb or greater. As indicated in Table 3, all measures for O_3 satisfy or nearly satisfy the EPA guidances of MNGE $\leq$ 35%, $-20\% \leq$ UPA $\leq$ 20%, and

Table 2
Definition of model performance statistics.

Parameter	Definition
Unpaired Peak Accuracy (UPA)	$\left(\frac{P^u_{\text{peak}} - O_{\text{peak}}}{O_{\text{peak}}}\right) \times 100\%$
Mean Normalized Gross Error (MNGE)	$\left(\frac{1}{N}\sum_{i=1}^{N}\left\lvert\frac{P_i - O_i}{O_i}\right\rvert\right) \times 100\%$
Mean Normalized Bias Error (MNBE)	$\left(\frac{1}{N}\sum_{i=1}^{N}\left(\frac{P_i - O_i}{O_i}\right)\right) \times 100\%$

P_i: prediction at time i; O_i: observation at time i; N: total number of observation; P^u_{peak}: maximum predicted concentration; O_{peak}: maximum observed concentration.

Author's personal copy

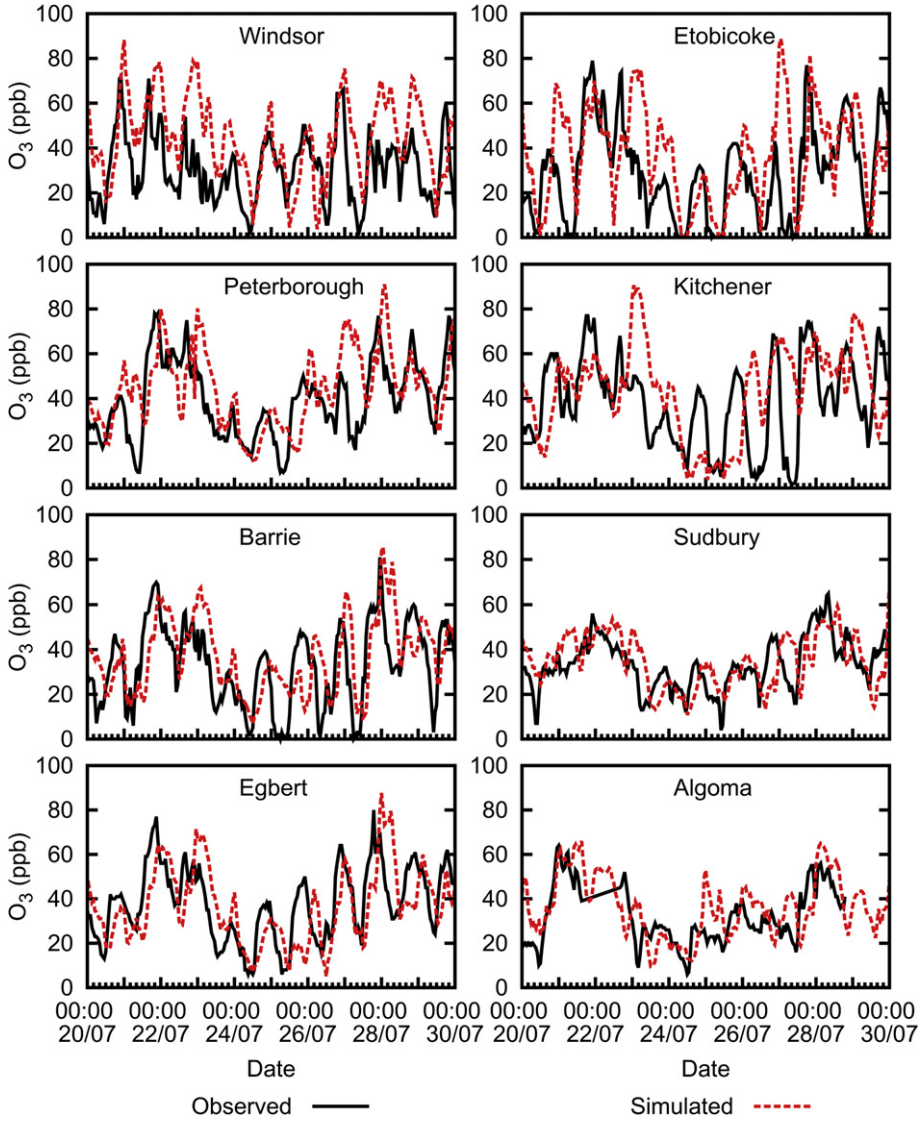

Fig. 4. Modeled (red dash) and measured (black solid) O_3 concentrations (ppb) for each test site during the simulation period from July 20th to 29th, 2002. (For interpretation of the references to colour in this figure legend, the reader is referred to the web version of this article.)

$-15\% \leq$ MNBE $\leq 15\%$ (U.S. EPA, 1991). They are also comparable to the values reported by other studies (Khiem et al., 2011; Goncalves et al., 2009; Korsakissok and Mallet, 2010), indicating satisfactory performance of the model in simulating O_3. The statistics also show that the modeled O_3 concentrations agree better for rural sites (Egbert and Algoma) or smaller towns (Sudbury, Barrie and Peterborough) than more polluted sites (Windsor, Etobicoke and Kitchener) located in or near big cities. We also compared observed and simulated O_x ($O_3 + NO_2$) because O_x is more conserved than O_3 due to the removal of NO titration effects. From UPAs and MNGEs in Table 3, we can see that the comparisons are obviously improved when the effects of NO titration are canceled out.

4.2.2. NO_x results

Hourly measured and modeled NO_x concentrations for six test sites are shown in Fig. 5. The two rural sites, Egbert and Algoma,

Table 3
Statistic for predicted O_3, NO_x, O_x($O_3 + NO_2$) concentrations.

Site	UPA (%)			MNBE (%)			MNGE (%)		
	O_3	NO_x	O_x	O_3	NO_x	O_x	O_3	NO_x	O_x
Windsor	22.5	24.7	12.9	14.7	7.2	21.3	30.5	62.5	28.9
Etobicoke	12.4	4.2	−17.5	−16.3	12.1	−1.2	29.7	70.4	25.1
Sudbury	4.8	−73.8	−0.5	−11.5	−73.8	−16.6	22.8	75.2	24.8
Peterborough	16.6	70.3	−3.0	−1.7	−61.7	−3.3	27.0	74.5	26.9
Barrie	5.7	−72.6	−0.6	−9.8	−67.0	−14.7	29.4	73.2	26.8
Kitchener	17.6	27.7	1.3	−9.5	−11.7	−8.7	34.8	85.6	29.9
Egbert	9.6			−13.7			29.1		
Algoma	3.0			−2.2			23.2		

Author's personal copy

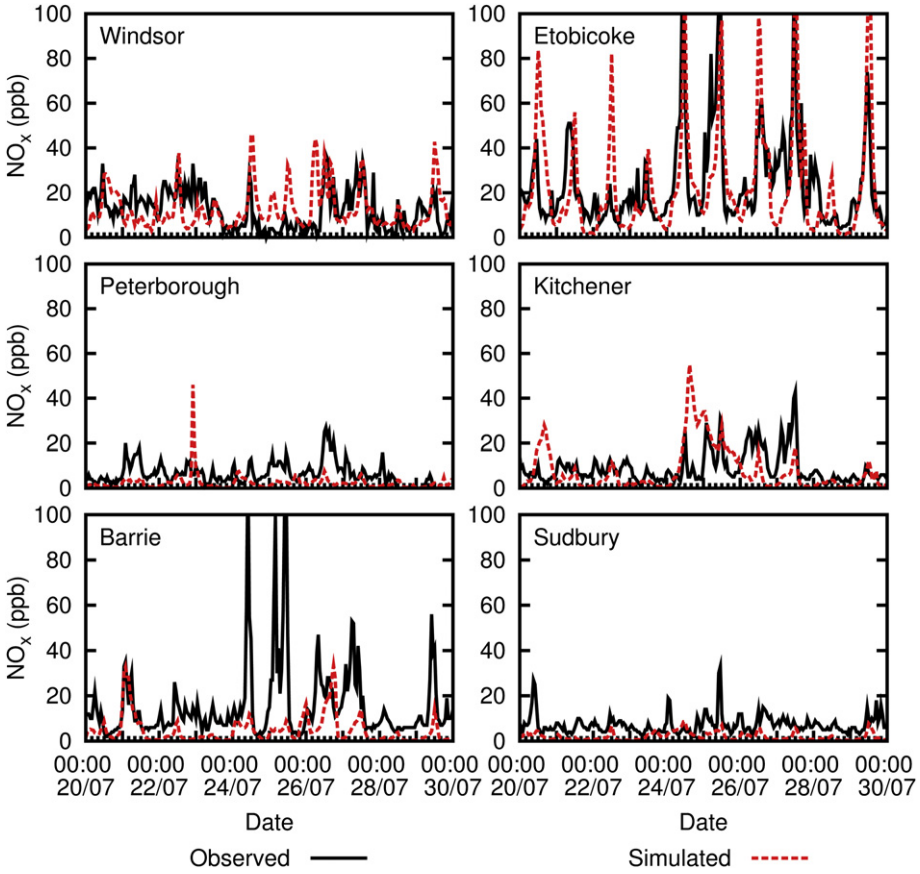

Fig. 5. Modeled (red dash) and measured (black solid) NO_x concentrations (ppb) for the six test sites during the simulation period from July 20th to 29th, 2002. (For interpretation of the references to colour in this figure legend, the reader is referred to the web version of this article.)

were not included due to their lack of NO_x measurements. The three performance metrics mentioned above were also calculated for NO_x, where a cut-off value of 5 ppb was used for the calculation of MNGE and MNBE. The resulting values are presented in Table 3.

As seen in Table 3 and Fig. 5, model performance for NO_x was much poorer than for O_3. For instance, MNGEs for NO_x are much higher than for O_3. The difficulties in simulating NO_x by air quality models are well-known, with other studies—e.g., Guerrero (2005); Biswas et al. (2001)—also exhibiting large errors that are similar in magnitude to the current study.

As indicated by the significant negative MNBE values of −60 to −70% at Sudbury, Peterborough, and Barrie, the model considerably under-predicted NO_x at these 3 sites. A tendency toward under-prediction of NO_x, especially by regional scale air quality models, is widely reported (Russell and Dennis, 2000; Lurmann and Kumar, 1997; De Leeuw et al., 1990; Lu et al., 1997; Hanna et al., 1996; Reynolds et al., 1996; Lin et al., 2008). One possible reason is the dilution of the NO_x plume over a whole gridcell by a gridded emission model, at horizontal resolutions coarser than the scale of NO_x plume. The severe under-estimation in this study was observed at Sudbury, Peterborough, and Barrie, all smaller cities/towns, in which NO_x may be elevated by relatively local sources that in the model are diluted over the horizontal spacing of 36 km in the NO_x emission grid—as indicated by the gridded emissions seen in Fig. 2. Case in point is Barrie, where a problem is clearly evident: NO_x concentrations are elevated above the simulated values, and numerous plumes are missed by the model (Fig. 5). A look at the Barrie station revealed that the site was located by a major highway prone to be affected by local, traffic-derived NO_x emissions.

In contrast, the bias is much smaller in larger urban areas—Windsor, Etobicoke, and Kitchener (Table 3). We suspect this is because in larger cities NO_x emissions are found over a wider area that are better represented by the emission grid. Moreover, photochemistry causes NO_x removal to be slower under NO_x-saturated conditions (Kleinman, 1994) while in low-NO_x areas chemical removal of NO_x is more efficient, exacerbating the under-prediction of NO_x for the sites in smaller towns where NO_x concentrations are already under-predicted from dilution of more local, sub-gridscale emissions. Uncertainties in the emission inventories are another likely source of relatively poor performance of the model for NO_x. However, the impact of errors in the emission inventories cannot be assessed here due to lack of knowledge about such errors.

Fundamentally, the degraded model performance for NO_x as compared to O_3 stems from the fact that O_3 varies at larger, regional scales whereas NO_x varies more locally due to the latter's strong point sources and shorter chemical lifetime (Logan et al., 1981).

Finally, potential measurement errors in NO_x may not be ruled out. The sites in this study measured NO_x with standard chemiluminescence monitors equipped with molybdenum oxide converters. An interference in the chemiluminescence monitor (U.S. EPA, 1975; Steinbacher et al., 2007; Dunlea et al., 2007) could result in an overestimation of the real values in measurements of NO_2 (Lamsal et al., 2008).

4.2.3. *Sensitivity to particle mixing parameterization*

Due to the imperfect "particle-in-grid" approach for mixing and redistributing chemical species between different Lagrangian particles (Sect. 2.6), we carried out a sensitivity study to examine its

Author's personal copy

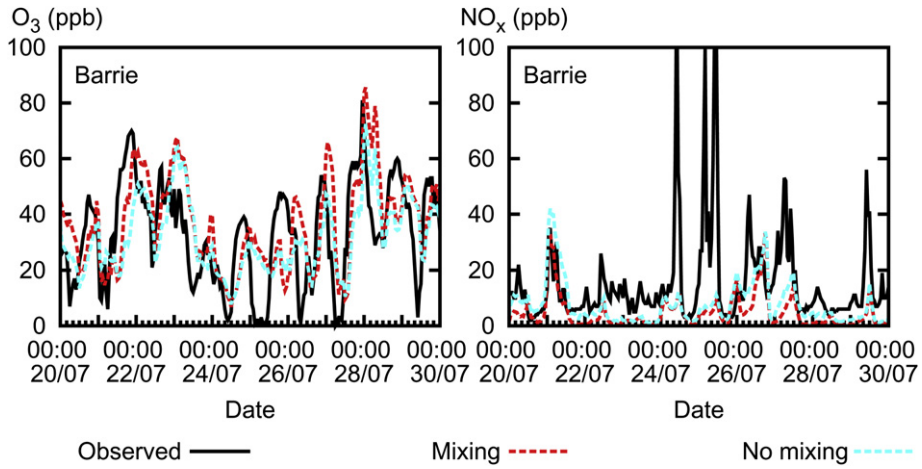

Fig. 6. Measured (black solid) and modeled O_3 and NO_x concentrations (ppb) at Barrie during the simulation period from July 20th to 29th, 2002. Modeled results include simulations with (red dash) and without (cyan dash) mixing and redistribution of chemical species between Lagrangian particles. (For interpretation of the references to colour in this figure legend, the reader is referred to the web version of this article.)

effect. To bracket the effect of mixing we added a simulation in which no particle mixing was implemented. In this simulation every single particle retained its own chemical identity, and no redistribution of chemical species with other particles was carried out at any point. Compared to the standard setup, in which perfect mixing occurred within individual gridcells, we expect the "true" mixing strength to be found between the two extremes of perfect mixing and no mixing.

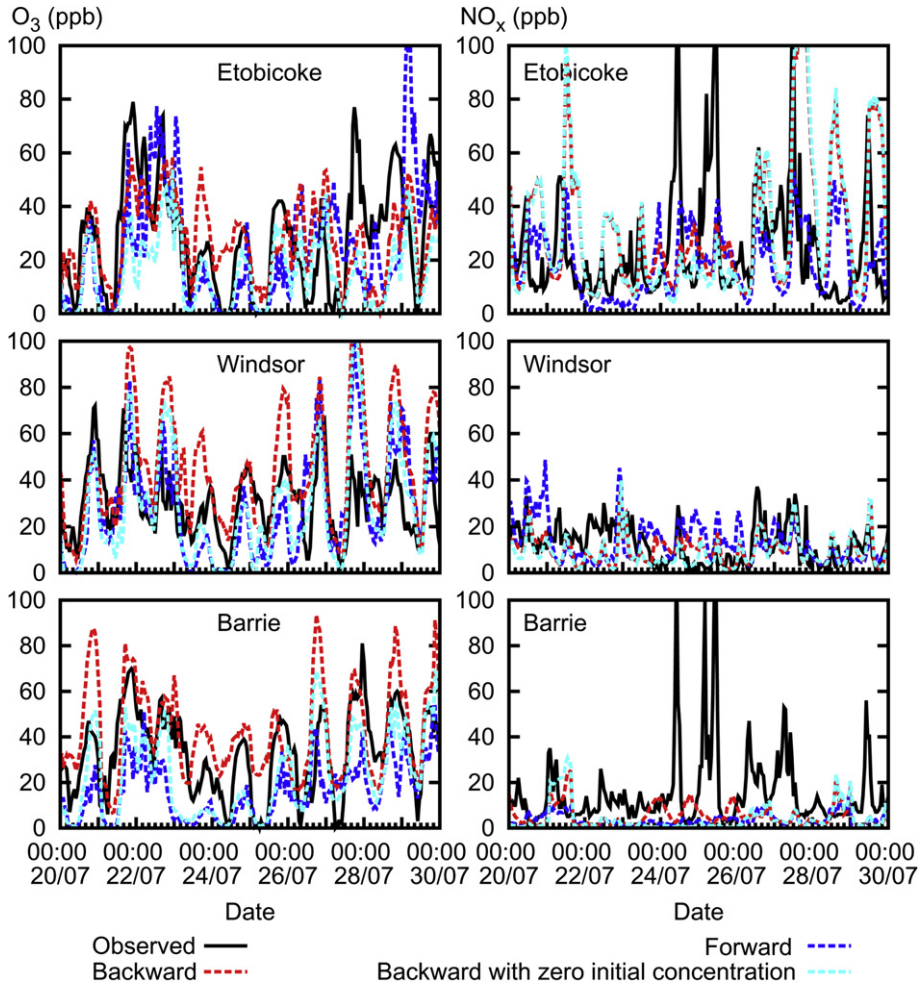

Fig. 7. Backward-modeled with initialization with GEOS-Chem output (red dash), backward-modeled with zero initial concentration (cyan dash), forward-modeled (blue dash) and measured (black solid) O_3 (Left) and NO_x (Right) concentrations (ppb) for Etobicoke (Top), Windsor (Middle), and Barrie (Bottom) during the simulation period from July 20th to 29th, 2002. (For interpretation of the references to colour in this figure legend, the reader is referred to the web version of this article.)

Author's personal copy

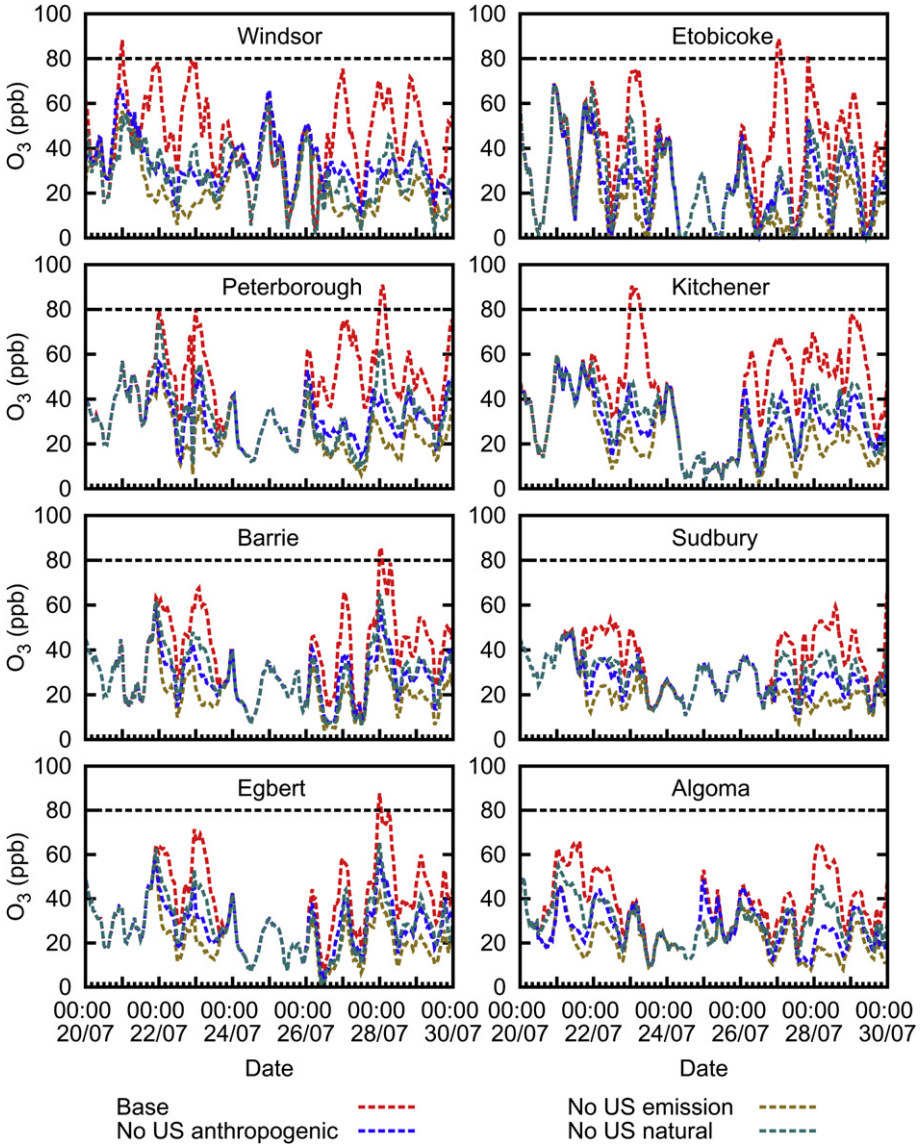

Fig. 8. Simulated O_3 concentrations for 1) base case (red); 2) No U.S. emissions (olive); 3) No U.S. anthropogenic emissions (blue); and 4) No U.S. natural emissions sources (teal) for each test site. The horizontal black dashed line denotes the one-hour ambient air quality criterion for Ontario (80 ppb). (For interpretation of the references to colour in this figure legend, the reader is referred to the web version of this article.)

Results are displayed in Fig. 6. It can be seen that differences between the two mixing algorithms were small. Indeed, one can conclude that discrepancies between the model and the observations, to first order, are likely not related to how mixing was implemented. Ideas regarding how to improve upon the mixing parameterization will be outlined in the Conclusions section.

4.2.4. Backward versus forward simulations

In order to examine the difference in simulation capabilities between a backward-time model and a forward-time model, we conducted two backward simulations using the model developed in this paper and a forward simulation using a previous approach (Stein et al., 2000).

It is important to point out that the forward and backward setups are not the same. In the forward simulation particles are emitted periodically throughout the model domain. The entire pollutant mass at each emission gridcell is uniformly distributed among the particles. These particles are then transported forward in time throughout the simulation domain. The concentration of each chemical species within a predefined concentration gridcell is calculated by dividing the sum of the particle masses of a particular chemical compound by the volume of the corresponding concentration gridcell in which the particles reside. The resulting concentrations are then utilized to calculate the new masses of the chemical species, which are assigned back to the particles within the cell. Once the redistribution has been performed, transport takes place again, followed by the computation of the chemical transformations and deposition for the next time step. New particles are released every time step from the sources to simulate fresh emissions of pollutants. Importantly, the forward setup did not include background contributions outside of the simulation domain through the initialization of particle concentrations using lateral boundary conditions (Stein et al., 2000). Instead, contributions solely from emissions within the simulation domain were accounted for in the forward simulations.

The simulation period runs from July 20th to 29th, 2002, for both backward and forward simulations. However, the forward simulation started two days earlier (July 18th) to allow

Author's personal copy

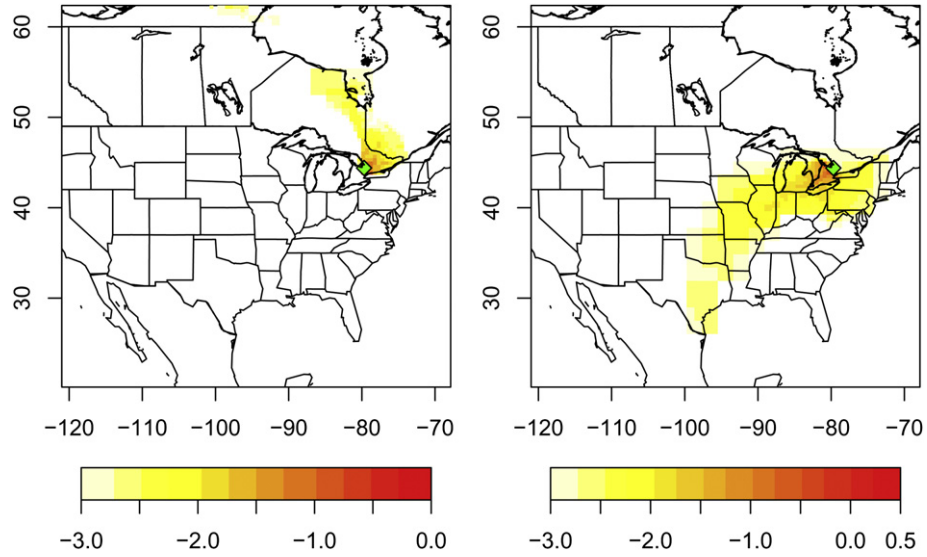

Fig. 9. Modeled footprint [$\log_{10}$(ppm (μmole m^{-2} s^{-1})$^{-1}$)] for Barrie for a period between July 24th to 25th showing northerly air flow from northern Canada (left), and a period between July 26th to 29th showing southerly air flow (right).

concentrations of the chemical species to be initialized. Thus, the first two-day results of the forward simulation were not used in result analyses. In the backward simulations, similar to the base case run, the particles were run backward in time for a period of 6 days. Two backward simulations were carried out to investigate the effect of concentration initialization on particles. One was initialized with the GEOS-Chem output, while the other was initialized with zero concentration to mimic the absence of background initialization in the forward simulation. The NARR meteorological data used for the base run were used for both backward and forward simulations. The same chemical mechanism, deposition method/parameters, photolysis method/parameters were also used for the both simulations. The forward model was originally configured to be driven with internally modeled deposition velocities (rather than outputted from MCIP) and an average diurnal cycle of gridded emissions (Stein et al., 2000). These modifications were implemented for the backward simulations in order to match the forward-model configuration in this comparison. The hourly-varying emission data were averaged over 20 days to generate an average diurnal cycle to serve as input for both simulations. Hence the backward simulations in this comparison differ from those shown in Figs. 4 and 5.

The modeled concentrations of O_3 and NO_x as well as measurements for Etobicoke, Windsor, and Barrie are displayed as an example in Fig. 7. Both the backward and forward simulations can reasonably capture the general trends and diurnal variation of O_3. However, there was a tendency toward under-prediction of O_3 concentrations by the forward simulations during July 24th to 25th, the period when concentrations are low and when northerly wind brought background air from higher latitudes (see Sect. 4.3, Fig. 9, and the accompanying text). The larger under-prediction is likely due to the lack of a mechanism to initialize background concentrations for particles in forward simulations. This is supported by the comparison between the forward simulation and the backward simulation initialized with zero concentration where the modeled concentrations are very close to each other when observed concentrations are low.

The concentrations of NO_x simulated by the forward model are comparable to those from backward modeling. NO_x was not obviously under-estimated by the forward simulation, mainly because NO_x, unlike O_3, is a more localized pollutant, and therefore is less significantly affected by the background level.

The comparison between the backward and forward simulations also demonstrated the computational efficiency of a backward simulation. The CPU time for each of the backward simulations is less than half of the time required by the forward simulation.

4.3. Model estimated contributions from U.S. sources

Exposure to elevated concentrations of ground-level O_3 is a serious health concern and adversely affects crops and living organisms in general (Chameides et al., 1994, 1999). Because Ontario is downwind of significant U.S. pollutant emissions that could affect its air quality, we examine here exactly how much U.S. emissions affect O_3 levels at different Ontario sites as an application of the backward-time stochastic Lagrangian air quality model. In order to investigate the cross-border transport of U.S. sources and their impact on Ontario, we conducted three different scenarios: 1) turning off U.S. anthropogenic sources; 2) turning off U.S. natural sources; 3) and turning off all U.S. sources (anthropogenic + natural sources). Only the impact on O_3 was examined here, as the NO_x simulations still contained the previously mentioned representation errors mainly caused by the dilution of emissions and the shorter chemical lifetime of NO_x (Fig. 5).

The modeled O_3 concentrations of the scenarios, along with the base case, are presented in Fig. 8. Almost all the sites demonstrate some time periods when O_3 concentrations were obviously affected ($C_{base} - C_{scenario} \geq 0.5$ ppb) by U.S. emission sources and some other

Table 4
Influence of U.S. sources on O_3 at the target sites during the July 20th to 29th, 2002 simulation period.

Site	Percentage of hours affected (%)			Max concentration of O_3 contributed (ppb)		
	A	N	T	A	N	T
Windsor	99	91	99	51.7	47.9	66.1
Etobicoke	72	73	78	61.5	63.7	80.0
Sudbury	56	58	60	33.8	28.6	49.4
Peterborough	66	66	68	52.2	56.9	68.8
Barrie	59	63	64	36.4	43.5	51.3
Kitchener	68	76	76	59.0	52.8	71.8
Egbert	61	64	65	37.5	41.7	51.5
Algoma	79	78	82	41.5	24.8	49.5

A: Anthropogenic emission, N: natural emission, T: Total emission.

Author's personal copy

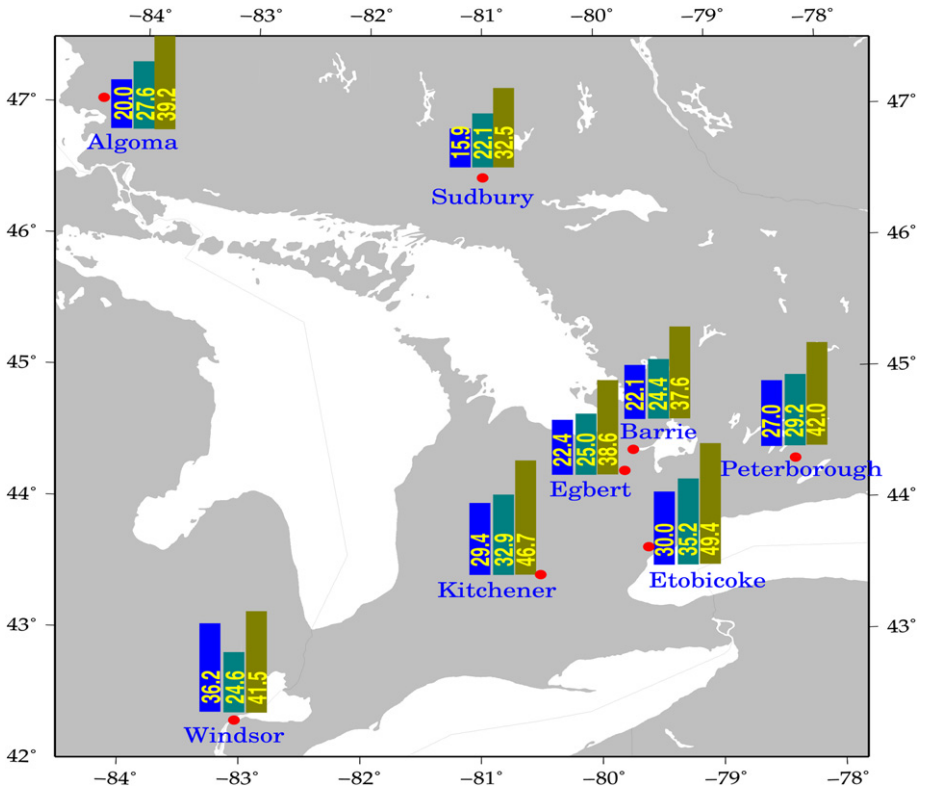

Fig. 10. Average percentage of O_3 concentrations contributed by: 1) U.S. natural emissions (blue bar); 2) U.S. anthropogenic emissions (teal bar); and 3) All U.S. emissions (olive bar) for each measurement site (red dot) during the simulation period. (For interpretation of the references to colour in this figure legend, the reader is referred to the web version of this article.)

periods not obviously affected ($C_{base} - C_{scenario} < 0.5$ ppb)—especially July 24th to 25th. To understand the different atmospheric transport between these periods, footprints during the two types of periods for Barrie are displayed as an example in Fig. 9. Footprints, which are deduced solely from air parcel trajectories, are indicated by the color scale. These show the sources of the air parcels detected during a period affected by U.S. sources and a period unaffected by them. Fig. 9 clearly shows that O_3 concentrations were significantly affected during July 26th to 29th due to the transport of pollutants from the U.S., while O_3 was not affected during July 24th to 25th due to relatively clean air flow from northern Canada.

The horizontal black dashed line in Fig. 8 denotes Ontario's one-hour provincial ambient air quality criteria (AAQC) for O_3 (OMOE, 2008), set to 80 ppb. Exceedances are found in the model for all of the sites except for the higher latitude sites of Sudbury and Algoma, albeit actual measurements indicated observed pollution episodes that were a few ppb short of the 80 ppb limit at Windsor, Peterborough, Etobicoke and Kitchener during this 10-day period (Fig. 4). Despite this model shortcoming, the difference between the red line (base) and all the other lines (different U.S. emissions switched off) clearly indicates significant influence of U.S. emissions on potential O_3 exceedances. The model results are suggestive that without contributions from U.S. natural or anthropogenic emissions, it is unlikely that O_3 concentrations would exceed the criteria level of 80 ppb at the study sites.

As presented in Fig. 8, the timing and length of periods affected by U.S. sources differ between sites. Table 4 shows the percentage of hours affected by U.S. sources, which indicates the relative significance of the contribution of U.S. sources to those sites. As expected, the percentage of hours affected in the simulation period depends on the transport distance to the U.S. border. O_3 concentrations at Windsor, the site closest to the U.S. border (right across from Detroit), were influenced almost all the time during the simulation period. Algoma has the second largest percentage of hours affected due to its short distance to the U.S. border. Sudbury and Barrie have the lowest percentages due to their longer transport distances. However, at all 8 sites over 50% of the hours are affected by U.S. emissions—either anthropogenic or natural.

Average percentages of O_3 concentrations contributed by different U.S. sources during the simulation period were calculated as another way to evaluate the extent of U.S. source contribution (Fig. 10). We can see that the contributions from U.S. natural sources are, in general, slightly smaller than anthropogenic sources except for only Windsor. We also can see that the contribution from total emissions is not a simple summation of contributions from each individual emission source, demonstrating non-linear impacts of emission sources. Sites like Windsor, Etobicoke, Kitchener and Peterborough are much closer to the U.S. border, and therefore they were subject to a more significant impact. For those sites, more than 24% of total O_3 was contributed from U.S. natural or anthropogenic sources, and total emission sources contributed more than 40% of O_3 concentration. Algoma, although very close to the U.S., was not affected as significantly because it is a rural site and situated in the north, where nearby U.S. emissions are low. U.S. sources have the least impact on Sudbury, again due to its long distance from the U.S. combined with the low U.S. emissions for that area.

Table 4 shows the maximum O_3 concentrations contributed from U.S. sources at each site during the simulation period. As expected, the maximum concentrations contributed are largest at the four sites close to the U.S. border in the south—Windsor, Etobicoke, Kitchener and Peterborough. Maximum O_3 concentration contributed from U.S. total emission sources were more than 66 ppb for those four sites and around 50 ppb for the other sites.

Author's personal copy

5. Conclusion and discussion

A backward-time stochastic Lagrangian air quality model was developed by incorporating the CB4 chemical mechanism into the STILT model. Thus, the model can use STILT to simulate the transport of air parcels backward in time and takes advantage of CB4 to simulate gas phase chemical transformations in the atmosphere along stochastic back trajectories. The capability for receptor-oriented chemical simulations based on stochastic particle trajectories significantly reduces the computational cost by limiting the model domain necessary for simulating and understanding tracer concentrations at receptors. The model was applied to eight measurement sites across Ontario, Canada, and evaluated against measured concentrations. The comparison demonstrated a satisfactory performance of the model for O_3, while NO_x is under-estimated at sites away from big cities. We suspect that the under-estimation is a consequence of the coarse-scale grid spacing for NO_x emissions, although artifacts in measurements of NO_x can also contribute to the discrepancy. Uncertainties in emission inventories are likely another source of the relatively poor performance of the model for NO_x.

One of the main difficulties in simulating chemistry in Lagrangian particle models is the parameterization of mixing between Lagrangian particles and the particle mass reassignment after chemical transformations. In this work, the particle-in-grid method was used for mixing and reassigning mass between particles. Although the particle-in-grid method is simple and easily implemented, it is still tied to Eulerian grids, preventing the model from taking fully advantage of the Lagrangian framework. Also, the particle-in-grid method lacks a physical basis in its mixing parameterization. Future studies will improve the parameterization of mixing by adopting a more sophisticated mixing scheme that is tied to the underlying physics. For example, the mixing scheme in the Chemical Lagrangian Model of the Stratosphere (CLaMS) (McKenna et al., 2002) introduces mixing between particles separated by distances below a critical value determined by the Lyapunov exponent of the atmospheric flow. The Lyapunov exponent is related to stretching of material surfaces and is thus closely associated to the physics of mixing (Ottino, 1989).

As an application of the backward-time stochastic Lagrangian air quality model, the cross-border transport and contribution of U.S. emission sources to receptor sites in Ontario, Canada, were examined. Model results suggest that total U.S. emissions contributed more than 30% of O_3 concentrations at all sites and anthropogenic emissions contributed a little more than natural emissions for most sites. Over half of all hours during the simulation period were affected either by anthropogenic or natural emissions from the U.S. sources. Furthermore, model results are suggestive that without U.S. emissions (either anthropogenic or natural) periods of O_3 exceedance above the 80 ppb criteria level would likely not take place at the sites. Although some uncertainties exist, the model results still provide indication of the significance of U.S. sources for air quality across Ontario.

Acknowledgment

D. Wen was supported by grants from Environment Canada and the Natural Sciences and Engineering Research Council of Canada J. Lin would like to thank Christoph Gerbig for helpful discussions regarding the backward-time approach to modelling atmospheric chemistry.

References

Aitken, A.C., 1932. On interpolation by iteration of proportional parts, without the use of difference. In: Proceedings of the Edinburgh Mathematical Society (Series 2), vol. 3, pp. 56–76.

Biswas, J., Hogrefe, C., Rao, S.T., Hao, W., Sistla, G., 2001. Evaluating the performance of regional-scale photochemical modeling systems. Part III—Precursor predictions. Atmospheric Environment 35, 6129–6149.

Brankov, E., Henry, R.F., Civerolo, K.L., Hao, W., Rao, S.T., Misra, P.K., Bloxam, R., Reid, N., 2003. Assessing the effects of transboundary ozone pollution between Ontario, Canada and New York, USA. Environmental Pollution 123, 403–411.

Brasseur, G.P., Orlando, J.J., Tyndall, G.S., 1999. Atmospheric Chemistry and Global Change. Oxford University Press, p. 654.

Byun, D.W., Pleim, J.E., Tang, R.T., Bourgeois, A., 1999. Meteorology-chemistry Interface Processor (MCIP) for Models-3 Community Multiscale Air Quality (CMAQ) Modeling System. US Environmental Protection Agency, Office of Research and Development, Washington, DC.

Canada CCME, 2000. Canada-wide Standards for Particulate Matter (PM) and Ozone. Canadian Council of Ministers of the Environment, Quebec City. http://www.ccme.ca/assets/pdf/pmozone_standard_e.pdf.

CEC, 2004. North American Power Plant Air Emissions, 87. Commission for Environmental Cooperation of North America, Montreal.

Chameides, W.L., Kasibhatla, P.S., Yienger, J., Levy, H., 1994. Growth of continental-scale metro-agro-plexes, regional ozone pollution, and world food production. Science 264, 74–77.

Chameides, W.L., Xingsheng, L., Xiaoyan, T., Xiuji, Z., Luo, C., Kiang, C.S., John, J.S., Saylor, R.D., Liu, S.C., Lam, K.S., Wang, T., Giorgi, F., 1999. Is ozone pollution affecting crop yields in China? Geophysical Research Letters 26, 867–870.

Chatfield, W.L., Delany, A.C., 1990. Convection links biomass burning to increased tropical ozone: however, models will tend to overpredict O_3. Journal of Geophysical Research 95 (D11), 18473–18488.

Chock, D.P., Winkler, S.L., 1994. A particle grid air quality modeling approach, 2. Coupling with chemistry. Journal of Geophysical Research 99 (D1), 1033–1041.

Chtcherbakov, A., 2003. Ontario Ministry of Environment, Personal communication.

Coats, C., 2003. The EDSS/Models-3 I/O API: User Manual. Baron Advanced Meteorological Systems. Available from: http://www.baronams.com/products/ioapi.

Crutzen, P.J., Ramanathan, V., 2000. The ascent of atmospheric sciences. Science 290, 299–304.

Davis, K.J., Lenschow, D.H., Oncley, S.P., Kiemle, C., Ehret, G., Giez, A., Mann, J., 1997. Role of entrainment in surface-atmosphere interactions over the boreal forest. Journal of Geophysical Research 102 (D24), 29219–29230. doi:10.1029/97JD02236.

De Leeuw, F.A.A.M., Van Rheineck Leyssius, H.J., Builtjes, P.J.H., 1990. Calculation of long term averaged ground level ozone concentrations. Atmospheric Environment Part A General Topics 24, 185–193. doi:10.1016/0960-1686(90)90455-V.

Draxler, R.R., Taylor, A.D., 1982. Horizontal dispersion parameters for long-range transport modeling. Journal of Applied Meteorology 21, 367–372.

Draxler, R.R., Hess, G.D., 1997. Description of the HYSPLIT 4 Modeling System. NOAA Technical Memorandum ERL ARL-224, 24.

Dunlea, E., Herndon, S., Nelson, D., Volkamer, R., SanMartini, F., Sheehy, P., Zahniser, M., Shorter, J., Wormhoudt, J., Lamb, B., 2007. Evaluation of nitrogen dioxide chemiluminescence monitors in a polluted urban environment. Atmospheric Chemistry and Physics 7, 2691–2704.

Eliassen, A., Saltbones, J., Hoy, O., Isaksen, I.S.A., Stordal, F., 1982. Lagrangian long-range transport model with atmospheric boundary layer chemistry. Journal of Applied Meteorology 21, 1645–1661.

Fitzjarrald, D.R., Lenschow, D.H., 1983. Mean concentration and flux profiles for chemically reactive species in the atmospheric surface layer. Atmospheric Environment 17, 2505–2512.

Gbor, P.K., Wen, D., Meng, F., Yang, F., Sloan, J.J., 2007. Modeling of mercury emission, transport and deposition in North America. Atmospheric Environment 41, 1135–1149.

Gear, C.W., 1971. Numerical Initial Value Problems in Ordinary Differential Equations. Prentice-Hall, Englewood Cliffs, NJ.

Georgopoulos, P.G., Seinfeld, J.H., 1986. Mathematical modeling of turbulent reacting plumes – I. General theory and model formulation. Atmospheric Environment 20, 1791–1807.

Gery, M.W., Whitten, G.Z., Killus, J.P., Dodge, M.C., 1989. A photochemical kinetics mechanism for urban and regional scale computer modeling. Journal of Geophysical Research 94 (D10), 12925–12956.

Gillani, N.V., Pleim, J.E., 1996. Sub-grid-scale features of anthropogenic emissions of NO_x and VOC in the context of regional Eulerian models. Atmospheric Environment 30, 2043–2059.

Goncalves, M., Jiménez-Guerrero, P., Baldasano, J.M., 2009. Contribution of atmospheric processes affecting the dynamics of air pollution in South-Western Europe during a typical summertime photochemical episode. Atmospheric Chemistry and Physics 9, 849–864. doi:10.5194/acp-9-849-2009.

Gourdji, S.M., Hirsch, A.I., Mueller, K.L., Yadav, V., Andrews, A.E., Michalak, A.M., 2010. Regional-scale geostatistical inverse modeling of North American CO_2 fluxes: a synthetic data study. Atmospheric Chemistry and Physics 10, 6151–6167.

Guerrero, P.J., 2005. Air Quality Modeling in Very Complex Terrains: Ozone Dynamics in the Northeastern Iberian Peninsula, Ph.D. Thesis, Polytechnical university of Catalonia.

Hanna, S.R., Moore, G.E., Fernau, M.E., 1996. Evaluation of photochemical grid models (UAM-IV, UAM-V, and the ROM/UAM-IV couple) using data from the Lake Michigan Ozone Study (LMOS). Atmospheric Environment 30, 3265–3279.

Jacobson, M.Z., 1998. Fundamentals of Atmospheric Modeling. Cambridge University Press, Oxford, UK, pp. 762.

Author's personal copy

Khiem, M., Ooka, R., Huang, H., Hayami, H., 2011. A numerical study of summer ozone concentration over the Kanto area of Japan using the MM5/CMAQ model. Journal of Environmental Sciences 23, 236–246.
Kleinman, L.I., 1994. Low and high NO_x tropospheric photochemistry. Journal of Geophysical Research 99, 16831–16838.
Korsakissok, I., Mallet, V., 2010. Development and application of a reactive plume-in-grid model: evaluation over Greater Paris. Atmospheric Chemistry and Physics 10, 8917–8931. doi:10.5194/acp-10-8917-2010.
Kort, E.A., Eluszkiewicz, J., Stephens, B.B., Miller, J.B., Gerbig, C., Nehrkorn, T., Daube, B.C., Kaplan, J.O., Houweling, S., Wofsy, S.C., 2008. Emissions of CH_4 and N_2O over the United States and Canada based on a receptor-oriented modeling framework and COBRA-NA atmospheric observations. Geophysical Research Letters 35, L18808. doi:10.1029/2008GL034031.
Lam, Y.F., Fu, J.S., 2009. A novel downscaling technique for the linkage of global and regional air quality modeling. Atmospheric Chemistry and Physics 9, 9169–9185. doi:10.5194/acp-9-9169-2009.
Lamsal, L.N., Martin, R.V., Donkelaar, A.V., Steinbacher, M., Bucsela, E., Dunlea, E.J., Pinto, J.P., 2008. Ground-level nitrogen dioxide concentrations inferred from the satellite-borne ozone monitoring instrument. Journal of Geophysical Research 113. doi:10.1029/2007JD009235.
Lin, J.C., Gerbig, C., Wofsy, S.C., Andrews, A.E., Daube, B.C., Davis, K.J., Grainger, C.A., 2003. A near-field tool for simulating the upstream influence of atmospheric observations: the stochastic time-inverted Lagrangian transport (STILT) model. Journal of Geophysical Research 108 (D16), 4493. doi:10.1029/2002JD003161.
Lin, J.C., Brunner, D., Gerbig, C., 2011. Studying atmospheric transport through Lagrangian models. EOS 92 (21), 177–184.
Lin, M., Oki, T., Bengtsson, M., Kanae, S., Holloway, T., Streets, D.G., 2008. Long-range transport of acidifying substances in East Asia–Part I: model evaluation and sensitivity studies. Atmospheric Environment 42, 5939–5955. doi:10.1016/j.atmosenv.2008.04.008.
Logan, J.A., Prather, M.J., Wofsy, S.C., McElroy, M.B., 1981. Tropospheric chemistry: a global perspective. Journal of Geophysical Research 86, 7210–7254.
Lu, R., Turco, R.P., Jacobson, M.Z., 1997. An integrated air pollution modeling system for urban and regional scales: 2. Simulations for SCACS 1987. Journal of Geophysical Research 102, 6081–6098.
Luginaah, I.N., Fung, K.Y., Gorey, K.M., Webster, G., Wills, C., 2005. Association of ambient air pollution with respiratory hospitalization in a government-designated "area of concern": the case of Windsor, Ontario. Environmental Health Perspectives 113 (3), 290–296.
Lurmann, F.W., Kumar, N., 1997. Evaluation of the UAM-V Model Performance in OTAG Simulations. In: Phase I: Summary of Performance against Surface Observations. Final Report No. STI-997250-1605-FR to Science Applications International Corp. Sonoma Technology, Inc., Santa Rosa, California.
Malig, B.J., Ostro, B.D., 2009. Coarse particles and mortality: evidence from a multi-city study in California. Occupational and Environmental Medicine 66, 832–839.
McKenna, D.S., Konopka, P., Grooß, J.U., Günther, G., Müller, R., Spang, R., Offermann, D., Orsolini, Y., 2002. A new chemical Lagrangian model of the stratosphere (CLaMS) 1. Formulation of advection and mixing. Journal of Geophysical Research 107 (D15), 4309.
Mesinger, F., DiMego, G., Kalnay, E., Mitchell, K., Shafran, P.C., Ebisuzaki, W., Jovi, D., Woollen, J., Rogers, E., Berbery, E.H., Ek, M.B., Fan, Y., Grumbine, R., Higgins, W., Li, H., Lin, Y., Manikin, G., Parrish, D., Shi, W., 2006. North American regional reanalysis. Bulletin of the American Meteorological Society 97, 343–360.
Miller, S.M., Matross, D.M., Andrews, A.E., Millet, D.B., Longo, M., Gottlieb, E.W., Hirsch, A.I., Gerbig, C., Lin, J.C., Daube, B.C., Hudman, R.C., Dias, P.L.S., Chow, V.Y., Wofsy, S.C., 2008. Sources of carbon monoxide and formaldehyde in North America determined from high-resolution atmospheric data. Atmospheric Chemistry Physics 8, 7673–7696. doi:10.5194/acp-8-7673-2008.
Millet, D.B., Guenther, A., Siegel, D.A., Nelson, N.B., Singh, H.B., de Gouw, J.A., Warneke, C., Williams, J., Eerdekens, G., Sinha, V., Karl, T., Flocke, F., Apel, E., Riemer, D.D., Palmer, P.I., Barkley, M., 2010. Global atmospheric budget of acetaldehyde: 3D model analysis and constraints from in-situ and satellite observations. Atmospheric Chemistry and Physics 10, 3405–3425.
Odman, M.T., 1997. A quantitative analysis of numerical diffusion introduced by advection alogrithms in air quality models. Atmospheric Environment 31, 1933–1940.
OMOE, 2008. Ontario's Ambient Air Quality Criteria. Available at: http://www.ene.gov.on.ca/stdprodconsume/groups/lr/@ene/@resources/documents/resource/std01 079182.pdf.
Ottino, J.M., 1989. The Kinematics of Mixing: Stretching, Chaos, and Transport. Cambridge University Press, Cambridge, UK, p. 364.
Pandey, M.D., Nathwani, J.S., 2003. Canada wide standard for particulate matter and ozone: cost-benefit analysis using a life quality index. Risk Analysis 23 (1), 55–67.
Press, W.H., Teukolsky, S.A., Vetterling, W.T., Flannery, B.P., 1992. Numerical Recipies: The Art of Scientific Computing. Cambridge University Press, New York.
Reynolds, S.D., Michaels, H., Roth, P., Tesche, T.W., McNally, D., Gardner, L., Yarwood, G., 1996. Alternative base cases in photochemical modeling: their construction, role and value. Atmospheric Environment 30, 1977–1988.
Russell, A., Dennis, R., 2000. NARSTO critical review of photochemical models and modeling. Atmospheric Environment 34, 2284–2324.
Russell, M., 1988. Ozone pollution: the hard choices. Science 241, 1275–1276.
Scire, J.S., Strimaitis, D.G., Yamartino, R.J., 2000. A User's Guide for the CALPUFF Dispersion Model (Version 5.0). Earth Tech, Inc., Concord, MA, p. 521.
Seibert, P., 2004. Inverse Modelling with a Lagrangian Particle Dispersion Model: Application to Point Releases over Limited Time Intervals. In: Air Pollution Modeling and Its Application, vol. XIV. 381–389.
Setzer, A.W., Pereira, M.C., Pereira, A.C., 1994. Satellite studies of biomass burning in Amazonia—Some practical aspects. Remote Sensing Reviews 10, 91–103.
Simpson, D., 1993. Photochemical model calculations over Europe for two extended summer periods: 1985 and 1989. Model results and comparison with observations. Atmospheric Environment 27A, 921–943.
Spellmann, J.W., Hindmarsh, A.C., 1975. GEARS: Solution of Ordinary Differential Equations Having a Sparse Jacobian Matrix. California University, Livermore Lawrence Livermore Laboratory, pp. 41.
Stein, A.F., Lamb, D., Draxler, R.R., 2000. Incorporation of detailed chemistry into a three-dimensional Lagrangian-Eulerian hybrid model: application to regional tropospheric ozone. Atmospheric Environment 34, 4361–4372.
Steinbacher, M., Zellweger, C., Schwarzenbach, B., Bugmann, S., Buchmann, B., Ordonez, C., Prevot, A.S.H., Hueglin, C., 2007. Nitrogen oxides measurements at rural sites in Switzerland: bias of conventional measurement techniques. Journal of Geophysical Research, D11307. doi:10.1029/2006JD007971.
Stevenson, D.S., Johnson, C.E., Collins, W.J., Derwent, R.G., Shine, K.P., Edwards, J.M., 1998. Evolution of tropospheric ozone radiative forcing. Geophysical Research Letters 25 (20), 3819–3822.
Stohl, A., 1998. Computation, accuracy and applications of trajectories - A review and bibliography. Atmospheric Environment 32, 947–966.
Stohl, A., Wotawa, G., 1995. A method for computing single trajectories representing boundary layer transport. Atmospheric Environment 29, 3235–3238.
Thompson, A., Pickering, K., Dickerson, R., Ellis Jr., W., Jacob, D., Scala, J., Tao, W.-K., McNamara, D., Simpson, J., 1994. Convective transport over the central United States and its role in regional CO and ozone budgets. Journal of Geophysical Research 99 (D9), 18703–18711.
Thomson, D.J., 1987. Criteria for the selection of stochastic models of particle trajectories in turbulent flows. Journal of Fluid Mechanics 180, 529–556.
Thomson, D.J., Physick, W.L., Maryon, R.H., 1997. Treatment of interfaces in random walk dispersion models. Journal of Applied Meteorology 36, 1284–1295.
U.S. EPA, 1975. Technical Assistance Document for the Chemiluminescence Measurement of Nitrogen Dioxide, Technical Report. Environmental Monitoring and Support Laboratory, U.S. Environmental Protection Agency, Research Triangle Park, NC 27711. EPA-600/4-75-003.
U.S. EPA, 1991. Guideline for Regulatory Application of the Urban Airshed Model, Office of Air and Radiation, Office of Air Quality Planning and Standards. Technical Support Division, Research Triangle Park, North Carolina, US. US EPA Report No. EPA-450/4-91-013.
U.S. EPA, 1997. National ambient air quality standards for ozone. Federal Register 62, 38855–38896.
U.S. EPA, 2004. 1999 National Emissions Inventory (NEI) Version 3 IDA Files. Available at: ftp://ftp.epa.gov/EmisInventory/finalnei99ver3/criteria/datafiles/.
U.S. EPA, 2007. Guidance on the Use of Models and Other Analysis for Demonstrating Attainment of Air Quality Goals for Ozone, PM2.5, and Regional Haze. US EPA, Research Triangle Park, NC 2771.
Vogelezang, D.H.P., Holtslag, A.A.M., 1996. Evaluation and model impacts of alternative boundary-layer height formulations. Boundary-Layer Meteorology 81, 245–269.
Walcek, C.J., 2002. Effects of wind shear on pollution dispersion. Atmospheric Environment 36 (3), 511–517.
Wen, D., Lin, J.C., Meng, F., Gbor, P.K., He, Z., Sloan, J.J., 2011. Quantitative assessment of upstream source influences on total gaseous mercury observations in Ontario, Canada. Atmospheric Chemistry and Physics 11, 1405–1415. doi:10.5194/acp-11-1405-2011.
Wesely, M.L., 1989. Parameterization of surface resistance to gaseous dry deposition in regional-scale numerical models. Atmospheric Environment 23, 1293–1304.
Yarwood, G., Rao, S., Yocke, M., Whitten, G., 2005. Updates to the Carbon Bond Chemical Mechanism: CB05. Final report to the US EPA, RT-0400675.
Zhao, C., Andrews, A.E., Bianco, L., Eluszkiewicz, J., Hirsch, A., MacDonald, C., Nehrkorn, T., Fischer, M.L., 2009. Atmospheric inverse estimates of methane emissions from Central California. Journal of Geophysical Research 114, D16302. doi:10.1029/2008JD011671.